PROTEINS
STRUCTURE ■ FUNCTION ■ BIOINFORMATICS

Solid-state NMR and simulation studies of equinatoxin II N-terminus interaction with lipid bilayers

Yuen Han Lam,[1] Andrew Hung,[2] Raymond S. Norton,[3] Frances Separovic,[4] and Anthony Watts[1]*

[1] Biomembrane Structure Unit, Department of Biochemistry, University of Oxford, Oxford OX1 3QU, United Kingdom
[2] School of Applied Sciences, College of Science, Engineering and Health, RMIT University, Victoria 3001, Australia
[3] The Walter and Eliza Hall Institute of Medical Research, 1G Royal Parade, Parkville, Victoria 3052, Australia
[4] School of Chemistry, Bio21 Institute, University of Melbourne, Victoria 3010, Australia

ABSTRACT

The interaction with model membranes of a peptide, $EqtII_{1–32}$, corresponding to the N-terminal region of the pore-forming toxin equinatoxin II (EqtII) has been studied using solid-state NMR and molecular dynamics (MD) simulations. The distances between specifically labeled nuclei in [^{19}F-para]Phe16-[1-^{13}C]Leu19 and [^{19}F-para]Phe16-[^{15}N]Leu23 analogs of $EqtII_{1–32}$ measured by REDOR in lyophilized peptide were in agreement with published crystal and solution structures. However, in both DMPC and mixed DMPC:SM membrane environments, significant changes in the distances between the labeled amino acid pairs were observed, suggesting changes in helical content around the experimentally studied region, 16–23, in the presence of bilayers. ^{19}F-^{31}P REDOR experiments indicated that the aromatic ring of Phe16 is in contact with lipid headgroups in both membrane environments. For the DMPC:SM mixed bilayers, a closer interaction between Phe16 side chains and lipid headgroups was observed, but an increase in distances was observed for both labeled amino acid pairs compared with those measured for $EqtII_{1–32}$ in pure DMPC bilayers. The observed differences between DMPC and DMPC:SM bilayers may be due to the greater affinity of EqtII for the latter. MD simulations of $EqtII_{1–32}$ in water, on a pure DMPC bilayer, and on a mixed DMPC:SM bilayer indicate significant peptide secondary structural differences in the different environments, with the DMPC-bound peptide adopting helical formations at residues 16–24, whereas the DMPC:SM-bound peptide exhibits a longer helical stretch, which may contribute to its enhanced activity against PC:SM compared with pure PC bilayers.

Proteins 2010; 78:858–872.

Key words: membranes; binding; phosphatidylcholine; sphingomyelin; surface properties.

INTRODUCTION

Equinatoxin II (EqtII) is a 179-residue, 19.8 kDa cytolysin isolated from the Mediterranean anemone *Actinia equina L.*[1] EqtII is a member of the family of actinoporins, which is characterized by a high pI, affinity for sphingomyelin, and permeabilizing activity of model and cell membranes.[2–6] EqtII is highly soluble in water, and its structure has been well characterized by X-ray crystallography and solution state NMR.[7,8] The structure consists of two short helices packed against opposite faces of a β-sandwich structure formed by a pair of five-stranded β-sheets. The core of the protein has extensive hydrophobic interfaces formed by residues projecting from the internal faces of the two β-sheets.

The N-terminal 32 residues, including an amphiphilic helix, adopt a different structure upon interaction with membrane bilayers,[9] but without disrupting the overall fold of the rest of the protein.[10,11] A cluster of exposed aromatic amino acid residues on the surface of EqtII, consisting of Tyr108, Trp112, Tyr113, Trp116, Tyr133, Tyr137, and Tyr138, is likely to have a role in membrane recognition and binding since aromatic residues have been shown to have affinity for the lipid–water interface.[12–14] CD and FTIR studies show small increases in β-sheet and α-helical content at the expense of random structure in the presence of unilamellar vesicles.[10,15–17] In principle, at least two steps are involved in formation of the EqtII pore, with initial binding of monomers to the membrane being followed by subsequent oligomerization into a functional pore. Site-directed mutagenesis has been used to show that at least

Abbreviations: DMPC, dimyristoylphosphatidylcholine; EqtII, equinatoxin II; MD, molecular dynamics; NMR, nuclear magnetic resonance; REDOR, rotational echo double resonance; SM, sphingomyelin; SS, solid-state.

Grant sponsors: The Medical Research Council (UK); The Australian Research Council.
*Correspondence to: Anthony Watts, Biomembrane Structure Unit, Department of Biochemistry, University of Oxford, Oxford OX1 3QU, United Kingdom.
E-mail: anthony.watts@bioch.ox.ac.uk.
Received 12 November 2008; Revised 31 August 2009; Accepted 1 September 2009
Published online 17 September 2009 in Wiley InterScience (www.interscience.wiley.com).
DOI: 10.1002/prot.22612

two regions of EqtII became embedded in lipid membranes, the N-terminal region (residues 10–28)[18] and the surface aromatic cluster including Trp112 and Trp116.[10,11,15,19] A model of the membrane-bound monomer envisages that the N-terminal helix involving residues 11–33, the hydrophobic region (residues 105–120), and Arg144, Ser160, and nearby residues, interact with the lipid membrane.[10] In the next step, the N-terminal helix translocates from the surface of the β-sandwich to the membrane, and finally traverses the lipid bilayer to form a cation-selective pore.[5,6,15]

Although these models suggest which regions of EqtII might interact with lipid membranes and undergo conformational changes to form the pore, little direct experimental evidence has been obtained concerning the conformational changes EqtII undergoes in reaching an oligomeric state, or during its incorporation into the target membrane. Recently, a series of peptides corresponding to the N-terminal region of EqtII has been studied and changes in secondary structure upon interaction with dodecylphosphocholine (DPC) micelles detected.[9] These studies indicate that the N-terminal peptide is sensitive to its environment, especially when a membrane surface (or mimetic) is present.

In this study, solid-state nuclear magnetic resonance (SS NMR) has been used to investigate the N-terminal domain of EqtII ($EqtII_{1–32}$) and its interaction with DMPC bilayers and DMPC:SM mixed bilayers. These serve as model systems to help elucidate the initial stages of membrane permeabilization by actinoporins. Molecular dynamics (MD) simulations have been applied to provide further atomic-level insight into the interactions between the $EqtII_{1–32}$ peptide, starting from a number of different initial conformations, and membrane bilayer models (DMPC and a mixed DMPC:sphingomyelin bilayer). MD simulations were also performed to study the interactions between EqtII placed initially in the water phase and a DMPC bilayer as a basis for comparison with our results on the N-terminal fragment peptide. Our computational simulations complement experimental studies; whereas, SS NMR data elucidate structural features of the final state of $EqtII_{1–32}$ interactions with DMPC and PC:SM membranes, MD simulations elucidate the structure, dynamics, and lipid contacts for the peptide and protein in the initial stages of interaction with the membranes. Additionally, a constrained simulation of the N-terminal fragment peptide on a DMPC bilayer with distance restraints derived from SS NMR provides further insights into the structure of the peptide.

MATERIALS AND METHODS

Materials

[^{19}F-para]Phe was purchased from Sigma-Aldrich (St Louis, MO) and [1-^{13}C]Leu and [^{15}N]Leu from Cambridge Isotopes (Andover, MA). [^{19}F-para]Phe16, [1-^{13}C]Leu19, and [^{15}N]Leu23 labeled N-terminal peptide of EqtII ($EqtII_{1–32}$) were supplied by Mimotopes (Melbourne, Australia) with purity >95% as determined by HPLC and MS. SM and DMPC were purchased from Avanti Polar Lipids (Alabaster, AL).

Sample preparation

Lipids (DMPC or DMPC:SM) were mixed in a chloroform/methanol (2:1; vol:vol) at 10 mg/mL in a round bottom flask. The solvent was removed using a rotary evaporator and the lipid mixtures were dried under high vacuum for 3–5 h. Lyophilized $EqtII_{1–32}$ was dissolved in water at a concentration of 5 mg/mL (pH ~6.5) and appropriate amounts used to give the desired toxin-lipid mole ratio (DMPC:SM:$EqtII_{1–32}$, 30:30:1 or DMPC:$EqtII_{1–32}$, 30:1). Each sample was subsequently put through five cycles of rapid freezing in liquid nitrogen and equilibration at 50°C. The multilamellar vesicle (MLV) suspensions were then concentrated in a Beckman benchtop centrifuge (28,000 rpm, 1 h, 4°C). The pellet (~100 μL) was loaded directly into a 4-mm NMR zirconia rotor for the magic angle spinning (MAS) NMR experiments.

Solid-state NMR spectroscopy

Heteronuclear distances were measured using REDOR[20,21] SS NMR on a CMX500 spectrometer (Chemagnetics, Varian, Palo Alto, CA). Samples were packed in 4-mm rotors and measured using a T_3 HFX MAS probe (Chemagnetics, Varian, Palo Alto, CA).

REDOR experiments were carried out in two steps: once with rotor-synchronized dephasing pulses (S_r) and once without (S_0). The dephasing pulse changes the sign of the heteronuclear dipolar coupling, and this interferes with the spatial averaging resulting from the motion of the rotor.[20,21] The difference in signal intensity ($\Delta S = S_0 - S_r$) for the observed spin is directly related to the corresponding distance to the dephasing spin. NMR data were analyzed using SIMPSON.[22] Heteronuclear distance measurements were carried out at room temperature on a lyophilized powder and at low temperature (−60°C) on membrane-bound peptide at 8 kHz spinning speed. Parameters used for ^{13}C-^{19}F REDOR experiments were as follows: recycle delay 14 s, 90° ^{1}H pulse width of 3.2 μs, ^{19}F 180° pulse 6.2 μs, ^{13}C 180° pulse 6.8 μs, 82 kHz TPPM decoupling power, dephasing time 0.5–20 ms, and the number of scans was 4–18 k and the XY-32 pulse phase cycling scheme was used. ^{13}C chemical shifts were referenced to hexamethylbenzene (HMB) at 17.36 ppm, and ^{19}F chemical shifts referenced to trifluoroethanol (TFE) at 0 ppm. For ^{31}P-^{19}F REDOR experiments, the parameters used were similar but with ^{19}F 180° pulse 7.1 μs and ^{31}P 180° pulse 7.5 μs. ^{31}P chemical shifts were referenced to 85% H_3PO_4 (0 ppm). For ^{15}N-^{19}F REDOR

experiments, similar parameters were used but with a 90° ^{1}H pulse width of 2.93 μs, ^{19}F 180° pulse 6.6 μs, and ^{15}N 180° pulse 8.65 μs. ^{15}N chemical shifts were referenced to saturated $^{15}NH_4Cl$ at 0 ppm.

Molecular dynamics simulation methodology

Molecular dynamics (MD) simulations were performed on $EqtII_{1–32}$ in the vicinity of DMPC and 1:1 ratio mixed DMPC and sphingomyelin (SM18:0) bilayers, with the systems solvated with SPC[23] water molecules and counterions included to ensure overall charge neutrality. A simulation was also performed on full-length EqtII in the vicinity of a DMPC bilayer as a comparison with the peptide SS NMR and MD simulation results. All MD simulations were performed using the program GROMACS version 3.1.4[24,25] under constant particle number, pressure, and temperature (NPT) conditions. The GROMOS96[24] force field with parameter set 43a1 were employed for all simulations. Lipid parameters for DMPC were adopted from Berger *et al.*[26] and those for sphingomyelin adopted from Chiu *et al.*[27] Temperature and pressure coupling were performed using the scheme described by Berendsen *et al.*[28] A constant pressure of 1 bar and pressure coupling constant of 1.0 ps were applied uniformly for the pure water systems, whereas for the bilayer simulations, separate pressure coupling was applied to the *xy*-plane and *z*-directions (i.e., the bilayer plane and normal, respectively). Water, DMPC, SM (for the mixed bilayer simulation), and protein were coupled separately to a temperature bath at 310 K with a temperature coupling constant of 0.1 ps. Electrostatic interactions were evaluated using the particle-mesh Ewald (PME) method[29] with van der Waals interactions truncated at 10 Å. Integration time steps of 2 fs were used. Bond lengths were constrained using the LINCS algorithm.[30] Analyses of MD trajectories were performed using the GROMACS suite of programs. Secondary structure analysis employed DSSP.[31] Visualization of system geometries and interactions and evaluation of protein secondary structure were performed using VMD.[32]

The simulation systems were set up as follows: for the full-length protein (labeled **prot-DMPC**), the atomic coordinates of the first monomer of the structure included in PDB file 1IAZ,[7] simulated in pure SPC water for 10 ns (no significant structural changes were evident; data not shown), were used as initial coordinates. The protein was placed initially ~20 Å above the headgroup region of the 288 lipid DMPC bilayer [initial structure in Fig. 6(g)] and simulated for 50 ns. For the $EqtII_{1–32}$/DMPC simulations, we used two different starting conformations and performed two separate unbiased simulations (i.e., no noncovalent distance constraints were applied). The first peptide simulation used the structure contained in BioMagResBank[33,34] with accession number 6808, labeled **pep-exp-DMPC** [Fig. 6(a)] and was simulated for 80 ns. The second peptide simulation used a structure obtained from a 10 ns simulation of the experimentally obtained structure in pure SPC water (data not shown), which produced significant loss of helicity at both termini [Fig. 6(d)]. This simulation is labeled **pep-wat-DMPC** and was also simulated for 80 ns. In both $EqtII_{1–32}$/DMPC simulations, the peptide was initially placed ~35 Å above a 128 lipid DMPC bilayer. Thus, two simulations with significantly different starting conformations were performed. Simulations using different starting conformations were used to enhance conformational sampling and improve the statistical relevance of any structural details and peptide-bilayer contacts revealed through the course of the simulations The **pep-exp** structure was chosen because it is the best known approximation of the structure of the peptide in a lipid-rich environment, whereas the **pep-wat** structure was chosen as an approximation of the peptide structure before contact with bilayers. Simulation of the latter structure enables examination of the binding mechanism of an initially fully solvated peptide to a bilayer surface. We also performed a distance-constrained simulation of $EqtII_{1–32}$, in which the initial structure was taken from the **pep-pdb-DMPC** simulation at ~50 ns at which the best fits to experimental distance measurements were obtained. Throughout the 10 ns simulation, distance constraints of 5 and 8.2 Å were enforced between Phe19 (sidechain H_ζ) and both Leu19 (backbone C) and Leu23 (backbone N), respectively. This simulation is labeled **pep-cons-DMPC** and was simulated for 15 ns. Applying constraints to an already equilibrated (i.e., stable) structure which possesses experimentally consistent inter-residue distances enables the study of the peptide structure that corresponds best to the SS NMR-determined structure in DMPC, while preventing introduction of large artificial biasing forces that might cause unphysical distortion of the peptide. This approach also enables examination of regions of the peptide other than those for which experimental measurements are available, while ensuring consistency with those same measurements.

For the $EqtII_{1–32}$/DMPC:SM bilayer simulation (labeled **pep-exp-mixed** simulated for 70 ns), the BMRB-6808 peptide structure was used as the starting structure, placed initially ~35 Å above a mixed DMPC:SM bilayer. The mixed bilayer is composed of 32 molecules of each lipid type on each bilayer leaflet and is generated from a pure DMPC bilayer by random replacement of DMPC with SM molecules. A subsequent 10 ns simulation run of the peptide-free mixed bilayer was performed, after which the final bilayer structure was acquired for the peptide-interaction simulation. An initial 100 ps solvent equilibration run with protein and lipid atoms positionally restrained for all simulations, followed by 100 ps of equilibration with protein atoms only restrained. This was followed between 50 (**prot-DMPC**) and 80 ns

(**peptide simulations**) of restraint-free (collection) simulations, the results of which we discuss in the following sections.

RESULTS AND DISCUSSION

Solid-state NMR

Heteronuclear distance measurements for lyophilized EqtII$_{1–32}$

Figure 1(a) shows the structure of EqtII and Figure 1(b) shows the structure of the N-terminus of EqtII$_{1–32}$ in DPC micelles, which is thought to represent a structure involved in an early step of membrane–protein interaction. Intermolecular distances for [^{19}F-para]Phe16-[1-^{13}C]Leu19 EqtII$_{1–32}$ and [^{19}F-para]Phe16-[^{15}N]Leu23 EqtII$_{1–32}$ pairs were determined by REDOR NMR. Figure 2(a–f) shows the ^{19}F-^{13}C REDOR of both dephasing and nondephasing spectra at rotor cycles 20, 40, 60, 80, and 90 of EqtII$_{1–32}$. Although there was only one ^{19}F label in the EqtII$_{1–32}$, spinning sidebands were observed at 8 kHz as ^{19}F has a relatively large chemical shift anisotropy (CSA) (~40 kHz). Figure 2(g) shows a dephasing curve of $\Delta S/S_0$ obtained with a best fit to the data. The [^{19}F-para]Phe16-[1-^{13}C]Leu19 distance obtained in lyophilized powder is in agreement with that measured in the crystal and solution structures of EqtII[7,8] (Table I). The distance for the pair [^{19}F-para]Phe16-[^{15}N]Leu23 in the EqtII structures (14.6 Å in the crystal and 12.9 Å in solution) is beyond the REDOR distance measurement limit.

Intermolecular distance measurements in DMPC membrane bilayers

Labeled EqtII$_{1–32}$ was added to DMPC bilayers at a molar ratio of 1 peptide to 30 lipids, with a hydration level of 50% w/v. To confirm that the sample was in a bilayer lamellar phase, a ^{31}P NMR spectrum with proton decoupling was obtained at 25°C. The spectrum (not shown) had CSA of −45 ppm, including a small isotropic component which was due to EqtII$_{1–32}$ disruption of the membrane bilayers. A similar result was reported previously for full-length EqtII.[37]

REDOR experiments were carried out at −60°C to eliminate the fast axial rotation of the peptide. Figure 3(a–c) shows ^{19}F-^{13}C REDOR spectra of [^{19}F-para]Phe16–[1-^{13}C]Leu19 EqtII$_{1–32}$ associated with DMPC bilayers. The signal decayed more rapidly than in the lyophilized form [Fig. 3(d)], implying that there was a significant decrease in the internuclear distance, which was determined to be 10.8 Å in the lyophilized form and 5.0 Å in DMPC bilayers (Table I). The distances between [^{19}F-para]Phe16 and [^{15}N]Leu23 EqtII are 14.6 and 12.9 Å in the X-ray and solution structures and are, therefore, beyond measurement by REDOR. The differences between distances in the crystal and solution structures may be due to the sensitivity of the conformation of the N-terminus

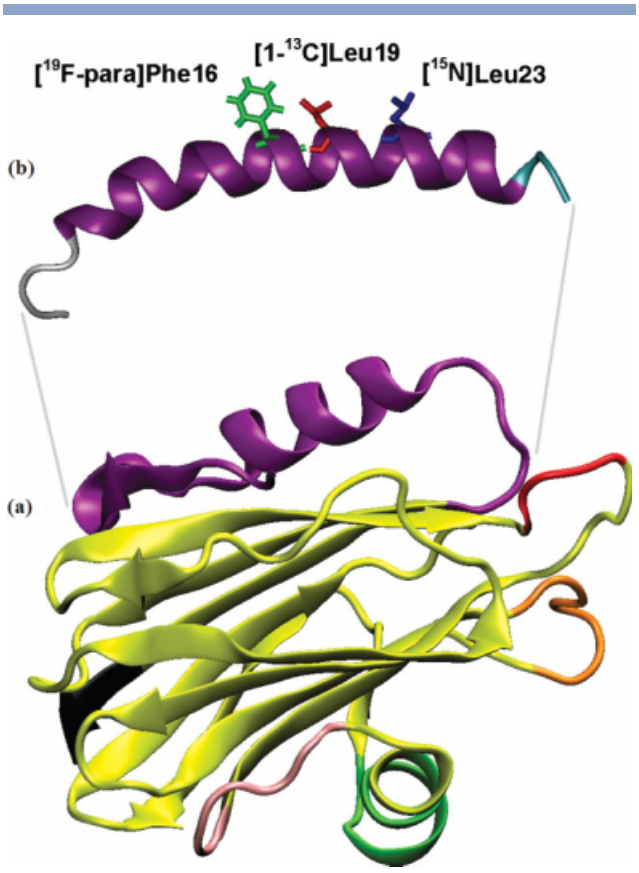

Figure 1

(**a**) Crystal structure of EqtII (PDB access code 1KD6) with two short helices (α1, residues 15–26, and α2, residues 129–134) packed against opposite faces of a β-sandwich type structure formed by a pair of five-stranded β-sheets, Arg79-81 are labeled in red, Tyr 108 –113 in orange; Lys123-Ala128 in pink; Glu134-Pro142 in green; Lys178-Ala179 in black, and (**b**) N-terminal domain EqtII$_{1–32}$ in DPC micelles (BMRB accession number 6808) with isotope labeling scheme as indicated. [Color figure can be viewed in the online issue, which is available at www.interscience.wiley.com.]

region of EqtII to pH and temperature. The pH was 4.6 and the temperature 100 K for the X-ray structure and 3.9 and 303 K for solution NMR.[8] When in the DMPC membrane environment, a notable change in the [^{19}F-para]-Phe16–[^{15}N]Leu23 distance from ~14.6 Å to 8.2 Å was observed by REDOR. A similar reduction in the [^{19}F-para]Phe16–[1-^{13}C]Leu19 distance (from ~10.9 Å to 5.0 Å) was also seen, indicating that the region from Phe16-Leu23 underwent a conformational change when the peptide interacts with DMPC bilayer membranes. This is possibly due to changes in the orientation of the Phe16 side chain or a change in secondary structure around this region. We have employed MD simulations to obtain further insight into these changes, as described below.

EqtII$_{1–32}$-DMPC headgroup contacts

Previous findings suggested that at least two regions of EqtII became embedded in lipid membranes, the

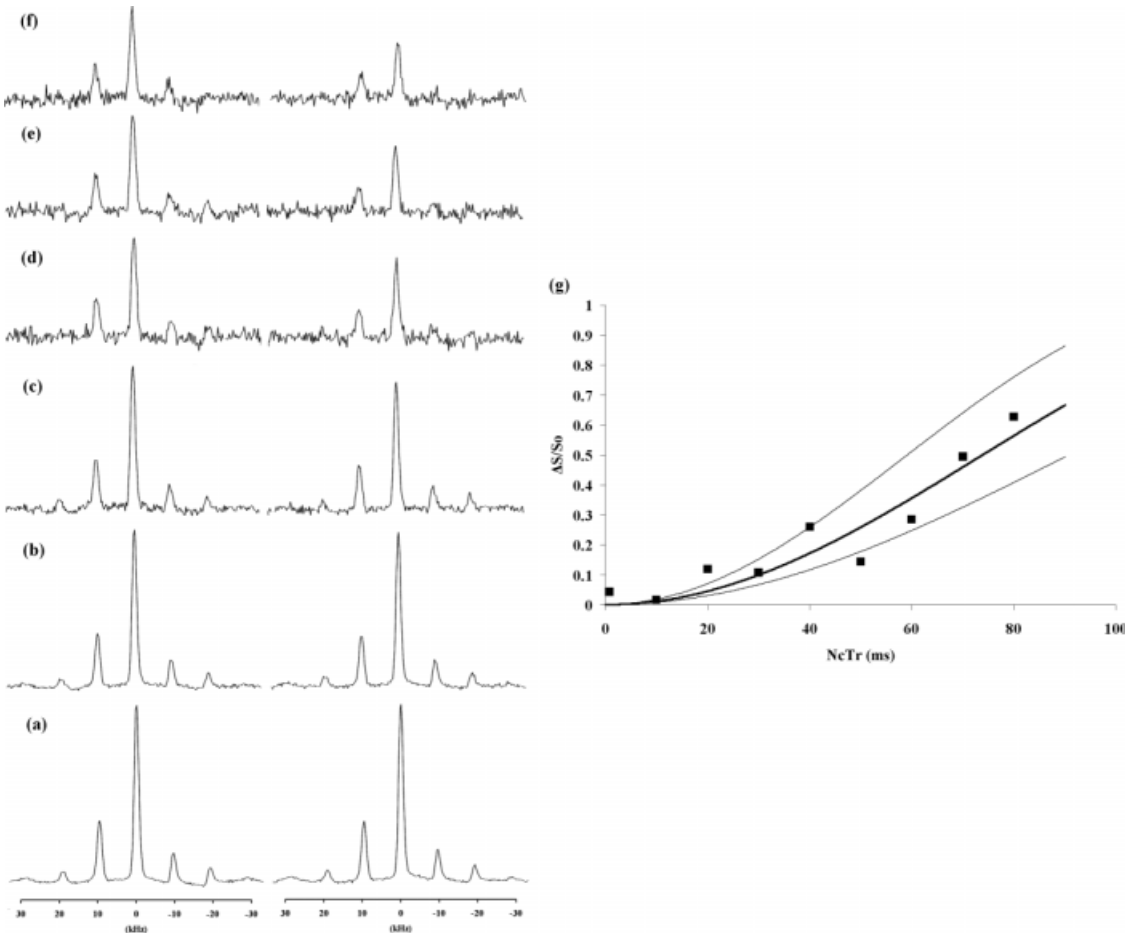

Figure 2

470.54 MHz ^{19}F-^{13}C REDOR full echo (S_0; left) and difference (S_D) spectra of 5 mg [^{19}F-para]Phe16-[1-^{13}C]Leu19 EqtII$_{1–32}$ as lyophilized powder after: (**a**) 20, (**b**) 30, (**c**) 40, (**d**) 60, (**e**) 80, and (**f**) 90 rotor cycles of dipolar evolution with MAS at 10 kHz. Each spectrum was the result of the accumulation of 4096 scans; and (**g**) ^{19}F-^{13}C REDOR dephasing ($\Delta S/S_0$) data are represented by the squares. The solid line shows the calculated dephasing curve for an isolated ^{19}F-^{13}C pair with dipolar couplings of 21.4 Hz.

N-terminal region (residues 10–28) and the surface aromatic cluster including Trp112 and 116.[15,18,38] To gain insight into the relative positions of the Phe side chains with respect to the phospholipid headgroups, ^{19}F-^{31}P REDOR experiments were performed on [^{19}F-para]Phe16 EqtII$_{1–32}$-[^{31}P]DMPC. Rapid dephasing of the ^{19}F peak resulted from close proximity ^{19}F-^{31}P contacts between the Phe side chain and the phospholipid headgroups. This provides direct evidence for the proximity of the Phe16 side chain of EqtII$_{1–32}$ to the bilayer phospholipid headgroups.

The precise conformation and orientation of the peptide relative to the bilayer, either on or penetrating into the bilayer, is currently unclear. Therefore, the orientation relative to the membrane normal was investigated using static ^{19}F NMR spectra with proton decoupling, for which an isotropic peak was observed with a linewidth of 500 Hz, whereas ^{19}F MAS spectra of peptide as a lyophilized powder exhibited a linewidth of ~1500 Hz (Fig. 4). These linewidths indicate that axial rotation of the Phe16 sidechain is rapid and suggests that the benzene ring of Phe16 is on the water side of the water-bilayer interface, rather than buried inside the bilayer, in which case a slower axial rotation would have been observed.

Internuclear distance measurements in DMPC:SM bilayers

SM in the membrane creates conditions for irreversible insertion and pore formation by EqtII.[5,6] More recent studies have shown that the coexistence of liquid ordered and disordered lipid phases favor membrane insertion of EqtII.[39–42] Here, EqtII$_{1–32}$ was incorporated into a mixture of DMPC:SM (1:1 molar ratio), in which maximum leakage by EqtII has been demonstrated.[39] An increase in

Table I
Intermolecular Distances (±0.5 Å for SS NMR Measurements[35]) Involving Phe16 of EqtII from X-Ray Crystallography,[7] Solution,[8] and Solid-State NMR Measurements and MD Simulations

Sample	XRD EqtII	Solution NMR $EqtII_{1-32}$	SS NMR lyophilized powder	SS NMR in DMPC	SS NMR in PC:SM	MD+ $EqtII_{1-32}$	MD+ EqtII in DMPC
[^{19}F-para]Phe16-[1-^{13}C]Leu19	10.8	10.8	11.0	5.0	6.4	8 ± 2 (e-PC) 8 ± 2(w-PC) 10 ± 2 (PC:SM)	7.0 ± 2
[^{19}F-para]Phe16-[^{15}N]Leu23	14.6	12.9	>	8.2	>	12 ± 2 (e-PC) 10 ± 2(w-PC) 14 ± 2 (PC:SM)	10 ± 2
[^{19}F-para]Phe16-[^{31}P]lipid	N/A	N/A	N/A	7.0	6.0	9 ± 3 (e-PC) 15 ± 3(w-PC) 11 ± 3 (PC:SM)	9 ± 2

All units in Å.
N/A, not applicable due to lack of lipid in XRD crystal, solution NMR in aqueous solution and solid-state NMR in lyophilized powder.
>, out of range, maximum range for ^{19}F-^{15}N distance measurement is ~8 Å[36].
+, averaged over final 20 ns of simulation trajectories. "e-PC" and "w-PC" indicate "pep-exp-DMPC" and "pep-wat-DMPC" systems, respectively, whereas "PC:SM" indicate "pep-exp-mixed" system (see text for details). Uncertainty given as ± standard deviation. MD data which fit within current SS NMR experimental uncertainty are underlined.

the [^{19}F-para]Phe16–[1-^{13}C]Leu19 distance from 5.0 to 6.4 Å was seen when the peptide was incorporated into DMPC/SM bilayers compared with DMPC bilayers (Table I). An increase in the [^{19}F-para]Phe16–[^{15}N]Leu23 distance to a more extended structure (out of the REDOR measurable range) was also observed when the peptide was incorporated into DMPC/SM compared with that in DMPC, that is, 8.2 Å (Table I). This suggests that the presence of SM in this system affects the secondary structure of the peptide. Distances within the segments 16–23 and 19–23 are consistent with helical structure, but an induced kink brings these distances closer when the peptide interacts with a membrane bilayer. This is discussed in the section below ("Molecular dynamics simulations").

$EqtII_{1-32}$-phospholipid headgroup contacts

In DMPC:SM mixed bilayers, two types of phospholipid headgroups are present. A ^{31}P proton-decoupled MAS spectrum was acquired in an attempt to resolve

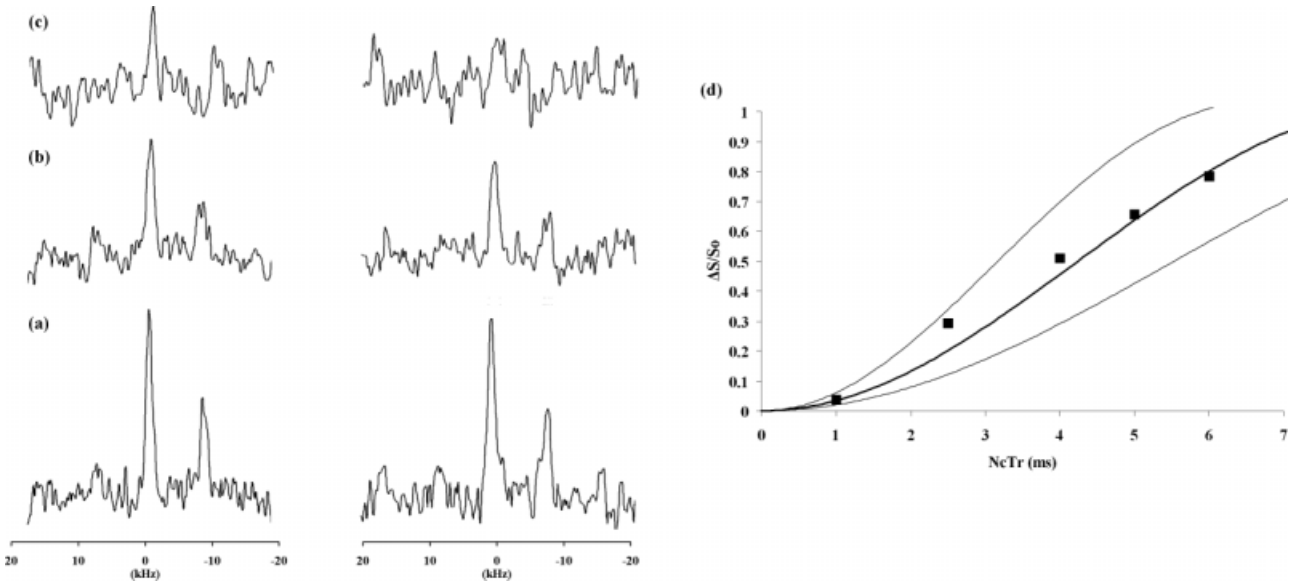

Figure 3
470.54 MHz ^{19}F-^{13}C REDOR full echo (S_0; left) and difference (S_D) spectra of 1 mg [^{19}F-para]Phe16-[1-^{13}C]Leu19 $EqtII_{1-32}$ incorporated in DMPC at lipid: peptide molar ratio of 30:1 after: (**a**) 4, (**b**) 12, and (**c**) 32 rotor cycles of dipolar evolution with MAS of 8 kHz and temperature −60°C; and (**d**) ^{19}F-^{13}C REDOR dephasing ($\Delta S/S_0$) data represented by the squares. The solid line shows the calculated dephasing curve for an isolated ^{19}F-^{13}C pair with dipolar couplings of 227.5 Hz.

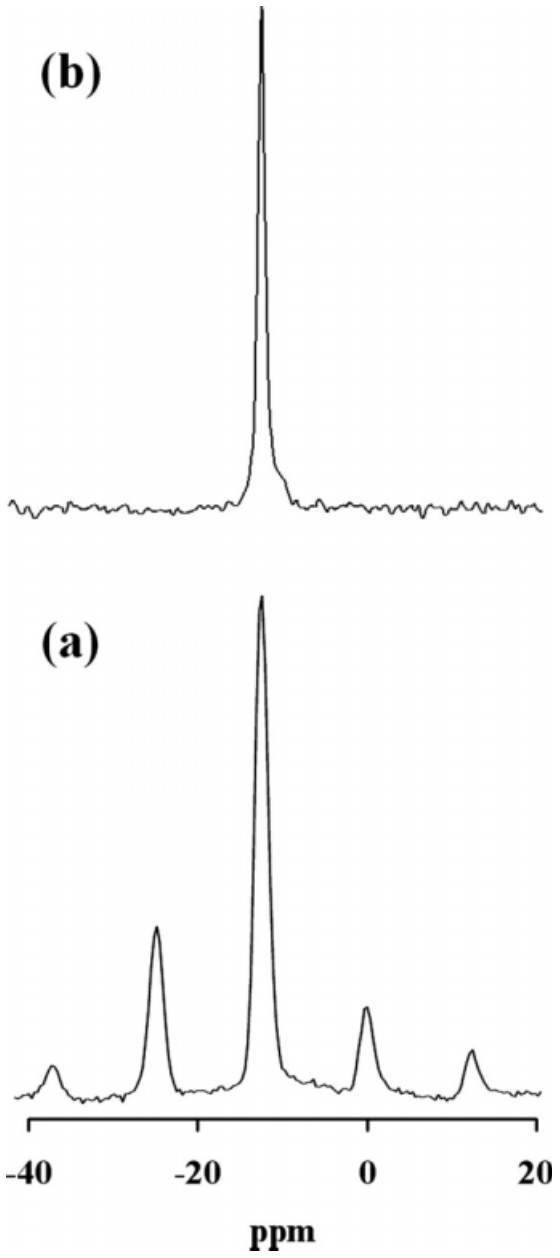

Figure 4

^{19}F spectra of [^{19}F-para]Phe16 EqtII$_{1–32}$ at 25°C as: (**a**) a lyophilized powder with MAS of 10 kHz, and (**b**) without spinning when incorporated into fully hydrated DMPC.

these two components, but at low temperature (−60°C), the linewidth of the ^{31}P peak increased and only one phosphorus component was seen. A ^{19}F-^{31}P REDOR experiment was performed on [^{19}F-para]Phe16 EqtII$_{1–32}$-[^{31}P]DMPC:SM, in which a reduction in distance between the peptide and phospholipid headgroups from 7.0 Å in DMPC to 6.0 Å in DMPC:SM was observed (Table I). Thus, the presence of SM brings the peptide and lipid closer together than in pure DMPC. Static ^{19}F NMR spectra of [^{19}F-para]Phe16 EqtII$_{1–32}$ incorporated into DMPC:SM at 25°C were similar to those in DMPC (data not shown), indicating that the Phe16 side chain is still located at the water interface.

Molecular dynamics simulations

EqtII$_{1–32}$ and EqtII structures and distances: comparisons with experiments

We have performed computational simulations on EqtII$_{1–32}$ and EqtII in the presence of lipid bilayers. For both the peptide and protein, we have also obtained structures by MD simulation in pure water. Simulation of EqtII$_{1–32}$ in water up to 10 ns revealed that the peptide in water adopts flexible loop and turn structures, in contrast to the helical structure seen in DPC micelles.[9] Inspection of the initial peptide conformation [Fig. 6(d)] for the **pep-wat-DMPC** simulation and the DSSP plot for this system at 0 ns [Fig. 5(b)] show that α-helicity is retained between residues 21–24, suggesting ~83% loss of the α-helical content compared with the DPC structure. This is consistent with previous NMR studies, which indicated that EqtII$_{1–32}$ in aqueous solution does not adopt an ordered conformation.[9] For full-length EqtII, there are no significant secondary structural changes during 10 ns simulation in water, although a higher degree of flexibility is observed in the N-terminal region (residues 1–15) relative to the rest of the protein (data not shown). This is consistent with previous NMR studies of EqtII,[8] which indicate the relative flexibility of the N-terminus.

For EqtII$_{1–32}$ and EqtII simulated in the presence of bilayers, average interatomic distances for Phe16-Leu19, Phe16-Leu23, and Phe16-P (calculated over the final 20 ns of the simulated trajectories, during which the peptide or protein maintains close contact with the bilayer surface throughout) and the associated standard deviations are given alongside experimentally determined values in Table I. Of the simulation data, the best fit to the SS NMR data are those of EqtII on DMPC (**prot-DMPC**), for which the lower limit of both Phe16-Leu19 and Phe16-Leu23 intramolecular interatomic distances fall within the experimentally determined range. All simulations (peptide and protein) produced Phe16-Leu19 distances that are statistically lower than those of the crystal and solution structures and lyophilized-power SS NMR experiments, in qualitative agreement with our current SS NMR experiments, which indicate a lowering of these values as a result of peptide interaction with DMPC. The Phe16-Leu23 distance for **prot-DMPC** and **pep-wat-DMPC** simulations are statistically lower than that obtained from the crystal and solution structures, also in qualitative agreement with the trend obtained from SS NMR. The **pep-exp-DMPC** simulation obtains a value lower than that of XRD but only marginally lower

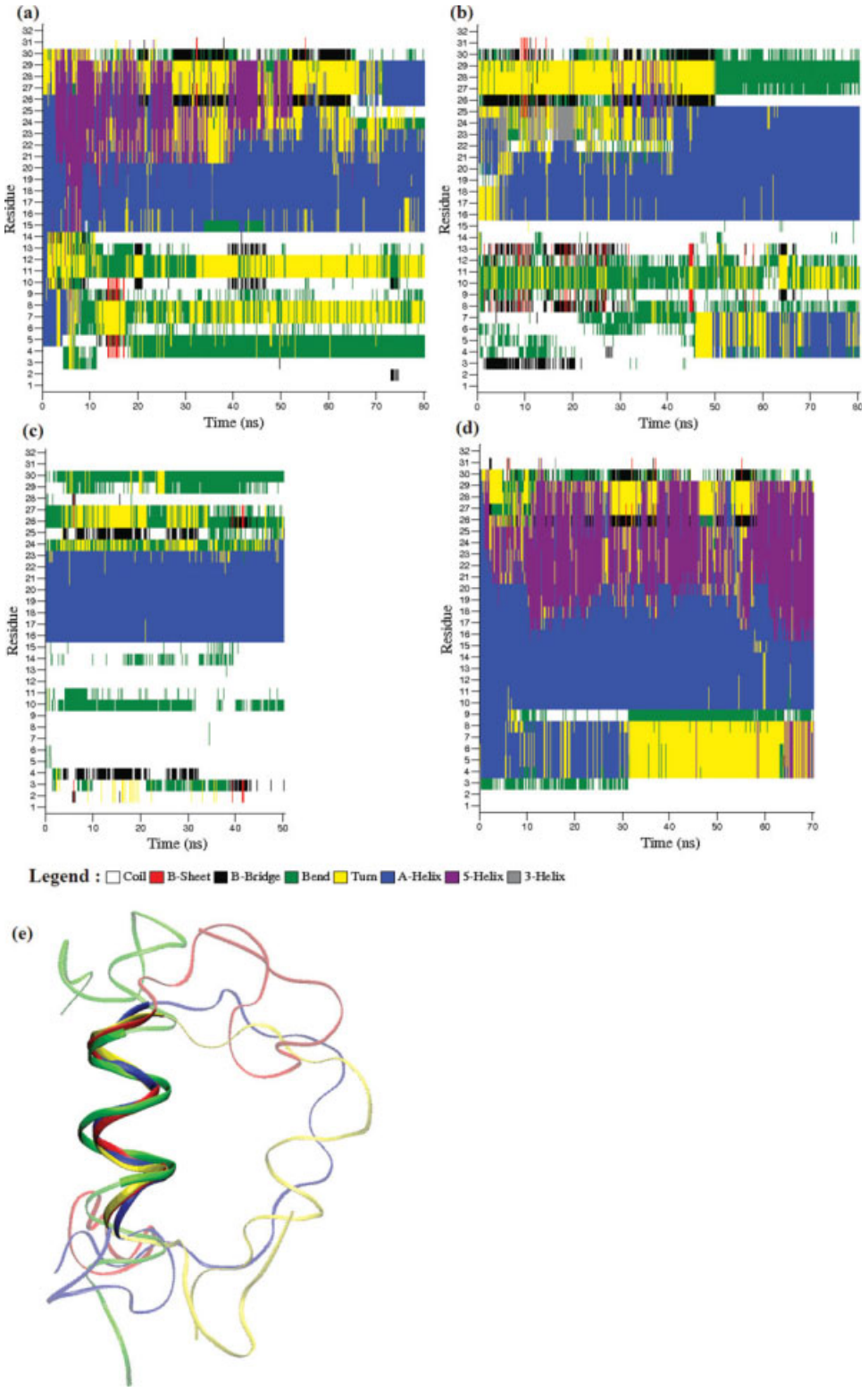

Figure 5

DSSP representations of secondary structure with respect to MD simulation time for: (**a**) pep-exp-DMPC, (**b**) pep-wat-DMPC, (**c**) prot-DMPC (residues 1–32), and (**d**) pep-exp-mixed. Secondary structures are differentiated by color, as defined in the figure legend. (**e**) Ribbon structures of residues 1–32 of the protein (blue), pep-exp-DMPC (red), pep-wat-DMPC (yellow), and pep-exp-mixed (green) obtained from the final snapshots of their respective simulations, overlayed via residues 16–24, which are shown as thicker ribbons.

than that obtained by solution NMR. Additionally, the Phe16-Leu19 distance for the peptide simulation on a mixed DMPC:SM bilayer (**pep-exp-mixed**) is higher than that obtained on a pure DMPC bilayer, with ~10 Å and ~8 Å, respectively. This is in qualitative agreement with SS NMR data, which indicate a longer Phe16-Leu19 distance (by 1.4 Å) in DMPC:SM compared with DMPC.

Overall, these distance data indicate that for the DMPC bilayer, the structure of $EqtII_{1–32}$ resembles the structure of residues 1–32 in the full-length protein, and thus lends some support to the N-terminal peptide as a valid model of the N-terminus of the full-length protein in membrane interaction studies. Furthermore, the simulations are consistent with our SS NMR results in so far as the Phe16-Leu19 and Phe16-Leu23 distances are reduced compared with the crystal and solution structures. However, quantitative agreement between constraint-free simulation and SS NMR for $EqtII_{1–32}$ was not obtained, possibly because of the disparity in the timescales between simulation (80 ns) and experiment (orders of magnitude longer). Nevertheless, the RMSD of the peptide backbone of all simulations plateaued at ~20 ns (data not shown), indicating that the simulations had reached equilibrium (i.e., were in local energy minima); furthermore, several distinct trends in peptide secondary structure and the mechanisms of initial bilayer interactions and subsequent binding were manifested in all of the simulations performed, discussed in subsequent sections. To obtain insights into the structure of the peptide while taking into account SS NMR-acquired distances, a distance-constrained simulation of $EqtII_{1–32}$ was performed in which Phe16(H_ζ) was distance-constrained at 5.0 and 8.2 Å to Leu19(C) and Leu23(N), respectively. Structural evolution for all systems simulated are discussed below.

Secondary structures

The secondary structural evolutions with respect to MD simulation time for $EqtII_{1–32}$ and EqtII are represented by DSSP plots (Fig. 5). For both **pep-exp-DMPC** and **pep-wat-DMPC** systems, the secondary structure feature that emerges is persistent helicity in the C-terminal half of the peptide (residues 16–24), with largely random-coil structures in the N-terminal half (residues 1 to 15). The emergence of similar secondary structural motifs after ~30 ns simulations for two peptide systems starting from different initial structures lends support to the notion that although the peptide is mainly unstructured in water (as observed in 10 ns simulation), the binding of the peptide to a DMPC bilayer produces structural bias toward helical forms in the C-terminal segment. This is consistent with experimental results for $EqtII_{1–32}$ in DPC micelles.[9] Inspection of the DSSP plot for residues 1–32 of **prot-DMPC** [Fig. 5(c)] indicates stability of secondary structural features throughout the 50 ns simulation. In agreement with the $EqtII_{1–32}$ simulations described earlier, residues 16–24 remain α-helical, whereas residues 1–15 are unstructured. Agreement between the secondary structure for $EqtII_{1–32}$ and the N-terminal segment of EqtII provides further support for the validity of using peptide fragments as experimental models of full-length actinoporin proteins. For the distance-constrained simulation **pep-cons-DMPC**, for which distance constraints were applied to maintain interatomic distances of 5 and 8.2 Å of Phe16(H_ζ) to Leu19(C) and Leu23(N), respectively, we find that the secondary structure does not change appreciably from that of the 50 ns "snapshot" of the **pep-exp-DMPC** structure, from which the initial **pep-cons-DMPC** structure was derived. This structure retains an α-helical segment between residues 16–23, a distorted helix between residues 24–29, and random coil between residues 1–15 [Fig. 6(l)], throughout the 15 ns simulation. The stability of the helical segments of the peptide in the presence of experimentally derived distance constraints lends further support to our (unbiased, constraint-free) MD simulations which indicate that the SS NMR-measured region of the peptide consists mainly of helix segments. It also indicates that the experimentally measured distances are consistent with a stable peptide structure.

Compared with the above simulations, different secondary structural behavior is observed for the 1:1 mixed DMPC:SM simulation, **pep-exp-mixed**, in which the initial structure is mainly α-helical (similar to that of **pep-exp-DMPC**). It exhibits greater structural stability relative to the peptide bound to DMPC as evidenced by the persistence of helical elements throughout the peptide between residues 10 and 29 [Fig. 5(d)], which is a much longer helical stretch than that exhibited by the peptide in the presence of DMPC only. There is a conformational transition at the N-terminal end (residues 1–9) to an extended β-strand after ~30 ns; unlike the DMPC simulations, very little random-coil structure is formed. The relative persistence (compared with DMPC alone) of helical and β-stranded secondary structure may be due to residue-dependent preference for interaction with either PC or SM, coupled with the structure of the underlying mixed bilayer "template," which forms distinct segregated nanometre-sized "domains" (i.e., small regions largely composed of either DMPC or sphingomyelin); the membrane thus imposes order on the peptide. More detailed discussions of peptide–lipid interactions are given in the next sections. The persistence of stable helicity throughout a larger portion of the peptide, together with the rapid formation of β-stranded N-terminus, may contribute to its enhanced activity against PC:SM bilayers compared with pure PC bilayers,[43] as the existing helix-strand motif may render the peptide more energetically favorable to bilayer permeation.

We note that that the N-terminal peptide structural characteristics are qualitatively consistent across all four

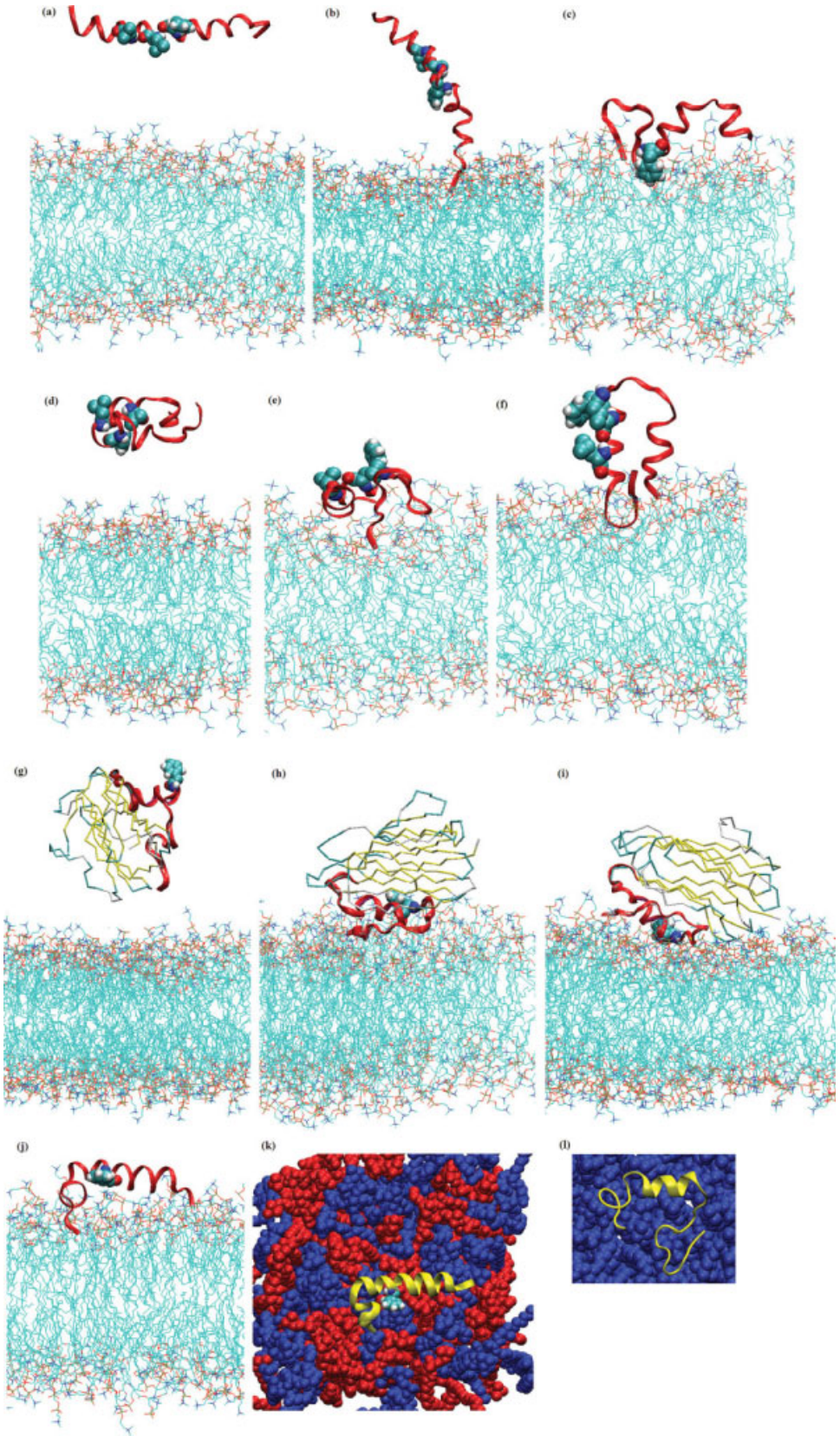

Figure 6

Representative structures of $EqtII_{1–32}$ and EqtII interactions with DMPC bilayers obtained as "snapshots" from MD simulation trajectories. Peptide backbone represented as red ribbons, Phe16, Leu19 and Leu23 represented in van der Waals' spheres, and lipids represented as thin lines. Atoms are colored as follows: cyan carbon, brown phosphorus, blue nitrogen, and red oxygen. (**a**) pep-exp-DMPC at 0 ns, (**b**) 1 ns, (**c**) 80 ns; (**d**) pep-wat-DMPC at 0 ns, (**e**) 20 ns, (**f**) 80 ns; (**g**) prot-DMPC at 0 ns, (**h**) 20 ns, (**i**) 50 ns; and (**j**) pep-exp-mixed at 70 ns viewed along axis perpendicular and (**k**) parallel to bilayer normal, with DMPC lipids represented as blue spheres, SM represented as red spheres, and the peptide backbone colored in yellow; (**l**) pep-cons-DMPC at 15 ns, viewed along bilayer normal, with DMPC lipids as blue spheres. [Color figure can be viewed in the online issue, which is available at www.interscience.wiley.com.]

of our simulations, with α-helical structure obtained in all four simulations between residues 16 and 24, and extended or random-coil structures at residues 1–15 and 24–32. The qualitative structural similarities are illustrated in Figure 5(e), which show the final snapshots of the peptide from the respective trajectories, overlayed by structural alignment of residues 16–24.

Interactions of EqtII$_{1–32}$ and EqtII with bilayers

Average interatomic distances for Phe16-P and the associated standard deviations for EqtII$_{1–32}$ and EqtII simulated with bilayers are given alongside experimentally determined values in Table I, calculated over the final 20 ns of the simulated trajectories for which the peptide or protein maintains close contact with the bilayer surface throughout. For the DMPC bilayer, the best fits to the SS NMR data are **pep-exp-DMPC** and **prot-DMPC**, consistent with visual inspection of these trajectories which indicate close contact between the Phe16 sidechain and the lipid surface [Fig. 6(c,i) respectively]. Likewise, inspection of the **pep-exp-mixed** trajectory indicate interactions between Phe16 and the bilayer [Fig. 6(j)], although specific close contacts between Phe16(H_ζ) and phosphorus are scarce. However, **pep-wat-DMPC** exhibited few close contacts between Phe16 and the bilayer surface; visual inspection confirms that the sidechain does not make close contact with the lipid headgroups throughout the 80 ns trajectory [Fig. 6(e,f)].

The total number of close contacts (defined as interatomic contacts below 0.35 nm) between the peptide/protein and the lipid bilayer atoms as a function of simulation time is given in Figure 7. All of the EqtII$_{1–32}$ simulations predict rapid association of the peptide with the bilayer surface, with **pep-exp-DMPC**, **pep-wat-DMPC**, and **pep-exp-mixed** forming peptide–bilayer contacts within 1 ns of simulations (Fig. 6). The contact-number plots reach a fluctuating plateau after ~40 ns, indicating saturation of peptide interactions with the bilayer surface (i.e., no further surface contacts are possible without significant peptide conformational changes). Visual inspection of the simulation trajectories reveals further details of the overall mechanism of interaction between EqtII$_{1–32}$ and EqtII with lipid bilayers. Figure 6 consists of "snapshots" of the simulation trajectories which serve to illustrate the overall dynamical behavior of the peptides and protein with respect to the membrane for the simulated systems. For the **pep-exp-DMPC** system, the initial contact between the peptide and bilayer is made via the N-terminus [Fig. 6(b)] and occurs within 1 ns. The helical segment of the peptide (residues 15–23; see above discussion on Secondary Structures) and the C-terminus subsequently form contacts with the lipid surface, with the helical segment lying at an incline of ~30° to the membrane normal [Fig. 6(c)]. A similar mechanism of binding is obtained for **pep-wat-DMPC**, which also interacts

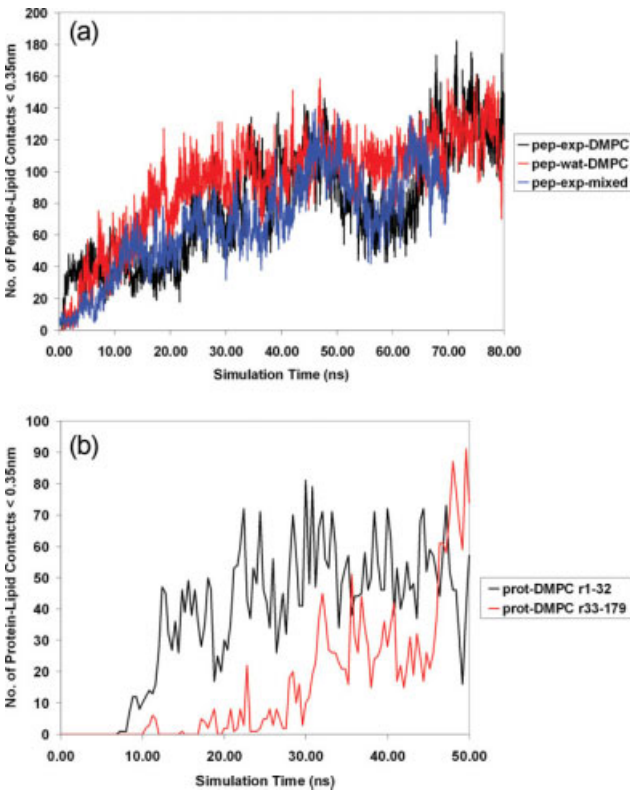

Figure 7

Total numbers of atomic contacts (<0.35 nm) between peptide and lipids with respect to MD simulation time for (**a**) pep-exp (black line), pep-wat (blue line) and pep-exp-mixed (red line) simulation systems, and (**b**) full-length EqtII, decomposed into contributions from residues 1 to 32 (black line) and 33 to 179 (red line). [Color figure can be viewed in the online issue, which is available at www.interscience.wiley.com.]

initially with, and inserts into the bilayer via the N-terminus, within 1ns. The C-terminus also binds to and inserts into the membrane surface at ~20 ns [Fig. 6(e)]. Interestingly, the helical segment of the peptide between residues 16 and 25, which adopts an orientation approximately parallel to the membrane plane upto ~60 ns, reorients after this point to adopt an "upright" orientation, with the helical axis roughly perpendicular to the membrane plane until the end of the trajectory at 80 ns [Fig. 6(f)]. Such a conformation may be suggestive of a "preinsertion" state of the peptide, in which the (potentially) pore-spanning helical segments adopt an orientation (tilt angle) similar to that of the fully inserted peptide, in preparation for membrane permeabilization.

Examination of the total number of contacts between each residue of the peptide with the phosphate headgroup and lipid carbon tails (averaged over the final 20 ns of trajectory) provides further details of the peptide's binding mechanism to the bilayer. Such "contact profile" bar graphs are shown in Figure 8. Figure 8(a) shows that significant contacts at both the N- and C-termini with lipid phosphate headgroups are made for both **pep-exp**

and **pep-wat-DMPC**, with the C-termini contacts maintained by the basic Lys30, Arg31, and Lys32. Basic sidechains are known to anchor membrane proteins to lipid bilayers via snorkeling interactions.[44] A number of additional contacts are formed for **pep-exp-DMPC**, at Ser13, Ser15, Phe16, and Lys20. Figure 8(b) shows the contact profiles for the peptides and the lipid carbon-tail atoms. There are far less numbers of atomic contacts, as none of the simulated peptides (and protein) penetrated the bilayer to any significant extent. However, in addition to the N- and C-termini, Gly11, Ala12, and Phe16 maintain contacts with the upper regions of the hydrophobic region of the bilayer.

We note that the relatively large fluctuations of peptide–lipid contact numbers for the **pep-exp-DMPC** simulation may be indicative of a relatively lower stability of the peptide–lipid binding orientation for this system compared with that of **pep-wat-DMPC**. The latter system exhibits relatively minor fluctuations in Figure 7(a) and is suggestive of "tighter" binding to the membrane surface. However, a significant result is obtained when we examine the DMPC trajectories to explain the apparent differences in binding orientation stability between the two simulations. Specifically, we note that there are greater numbers of contacts between Ser1, Asn28, Lys30, and Arg31 and the bilayer surface for the lower fluctuation, "more stable" **pep-wat-DMPC** simulation [Fig. 8(a)]. Both Asn28 and Arg31 also penetrate deeply into the bilayer in **pep-wat-DMPC**, making contacts with hydrophobic lipid chains [Fig. 8(b)]. The "less stable" **pep-exp-DMPC** simulation, in contrast, exhibits no significant sidechain insertions into the hydrophobic region of the bilayer at the C-terminus [Fig. 8(b)]. This suggests that close contact between the C-terminal residues—in particular, Asn28 and Arg31—and the bilayer enhances the strength of interaction between the peptide and the membrane, effectively anchoring the peptide to the membrane surface and resulting in a more stable binding mode (as in **pep-wat-DMPC**), while lack of these interactions results in greater orientational mobility of the peptide on the bilayer surface, as manifested in the **pep-exp-DMPC** simulation. This is consistent with the known preferential location of Arg at the lipid–water interface region in membrane proteins, in which the chemical structure of its sidechain enables it to form "snorkeling" interactions (e.g., Ref. [44]). Thus, despite the relatively large fluctuation in the peptide–lipid contact numbers time series for **pep-exp-DMPC**, the combined results of the **pep-exp** and **pep-wat-DMPC** simulations serve to highlight the potentially

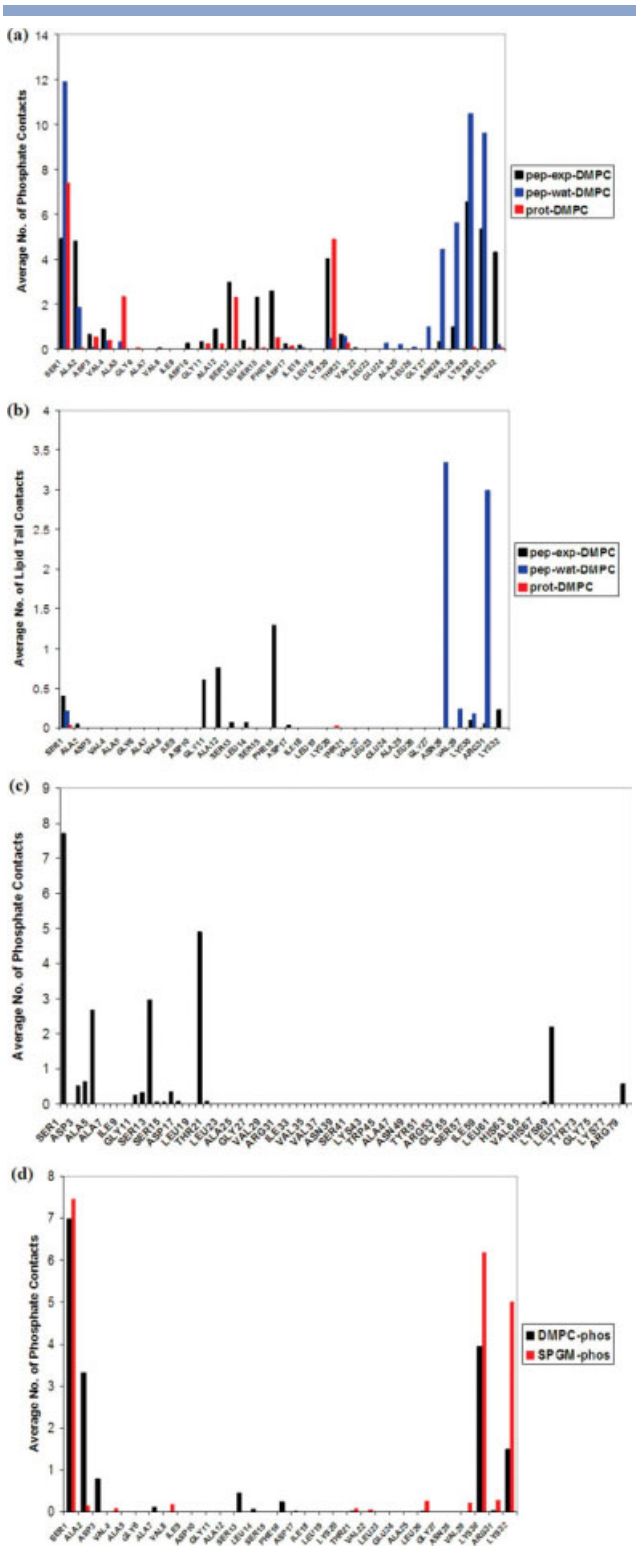

Figure 8

Numbers of atomic contacts (<0.35 nm) between each residue of $EqtII_{1-32}$ or EqtII and lipids, averaged over the final 20 ns of simulation trajectories. Residue-specific lipid contact profiles for (**a**) lipid phosphate group atoms and peptide for pep-exp (black bars), pep-wat (blue bars), and residues 1–32 of full-length protein (red bars); (**b**) lipid carbon-tail atoms and peptide for pep-exp (black bars), pep-wat (blue bars), and residues 1–32 of full-length protein (red bars); (**c**) lipid phosphate group atoms and residues 1–79 of EqtII (residues 80–179 exhibited negligible contacts); and (**d**) the $EqtII_{1-32}$ peptide residue-specific contacts with lipid phosphate group atoms from DMPC (black bars) and SM (red bars). [Color figure can be viewed in the online issue, which is available at www.interscience.wiley.com.]

important roles of charged sidechains such as Lys and Arg in imparting stability to the binding orientation of the peptide to DMPC membrane surfaces. A similar argument may be applied to **pep-exp-mixed** (mixed composition DMPC:SM bilayer), whose peptide–lipid contact plot also exhibits large fluctuations between 40 and 70 ns relative to **pep-wat-DMPC**, but somewhat lower fluctuations compared with **pep-exp-DMPC**. **Pep-exp-mixed** exhibits no sidechain penetration into the hydrophobic regions of the bilayer, unlike **pep-wat-DMPC**; hence, the former's lower binding stability and greater peptide–lipid contact number fluctuation. However, **pep-exp-mixed** exhibits greater numbers of contacts between Lys30/32 and headgroup phosphates compared with **pep-exp-DMPC**, which may result in marginally greater binding stability for the former. Thus, the binding stability of the peptide on the mixed bilayer is intermediate between that of the two DMPC simulation systems.

Protein–lipid contact plots for the EqtII protein are given in Figure 7(b), decomposed into contributions from residues 1–32 of the protein and residues 33–179 (i.e., the "remainder") of the protein. The plot indicates rapid association of the N-terminal, $r_{1–32}$ fragment of EqtII with the bilayer surface, with contacts formed with the membrane within ~5 ns (we note that the slower time to initial contact for the protein compared with the peptide is likely due to the slower diffusional motion of the former). The remainder of the protein (r33–179) forms few, nonpersistent contacts between 20 and 30 ns, with more significant numbers of contacts formed only after 30 ns of simulations. This indicates that the $r_{1–32}$ segment of the protein is strongly attracted to the bilayer surface, more so than other segments of EqtII. Indeed, visual inspection of the **prot-DMPC** trajectory [snapshots shown in Fig. 6(g–i)] reveals that, while the initial orientation of the protein is placed such that the long axis of the $r_{1–32}$ segment lies nearly parallel to the membrane normal [Fig. 6(g)], the protein undergoes rapid rotational and translational motion which results in the placement of $r_{1–32}$ directly in contact with the membrane, with the long axis aligned approximately perpendicular to the membrane normal [Fig. 6(h)]. Furthermore, between 40 and 50 ns, the helical segment at residues 14–23 is tilted to the bilayer normal at ~70° [Fig. 6(i)]. This coincides with the formation of new contacts between other regions (residues 69 and 79; see below) of the protein with the bilayer. Thus, **pep-exp-DMPC**, **pep-wat-DMPC**, and **prot-DMPC** all indicate that the short helical fragment around this region is oriented at an incline to the membrane surface.

A contact profile bar graph of the $r_{1–32}$ segment of EqtII superimposed on the $EqtII_{1–32}$ simulations [Fig. 8(a), red bars] indicates some similarities in the profile of residue-dependent contact with the phosphate headgroup atoms of DMPC; similar to both **pep-exp-DMPC** and **pep-wat-DMPC**, the protein makes significant headgroup contacts at the N-terminus. There are also significant contacts between Lys20 and phosphates. However, unlike the peptides, there are no significant contacts between the region around Lys32 (i.e., the C-terminus of $EqtII_{1–32}$) and phosphates, since this segment is bound to the remainder of the full-length protein. Since the protein is known to exhibit greater biological activity than the N-terminal fragment peptide,[2,3,9] significant binding between the (Lys32) C-terminus and the lipid headgroup region may be one factor which limits $EqtII_{1–32}$ membrane activity. We note that there are no significant contacts between any residue of the full-length protein and the hydrophobic region of DMPC [Fig. 8(b)]. This is in agreement with fluorescent studies, which suggest that EqtII does not insert deeply in the bilayer.[19] An extended contact profile graph for EqtII over residues 1 to 80 is shown in Figure 8(c) (residues 81 to 179 exhibited no contacts with the bilayer during this simulation; data not shown), indicating significant bilayer interactions at the N-terminal ($r_{1–32}$) segment and isolated interactions via Lys69 and Arg79. The latter two interactions are formed later in the simulation (40–50 ns).

The plot of the total number of contacts between the $EqtII_{1–32}$ peptide and a mixed 1:1 DMPC:SM bilayer [Fig. 7(a)] shows rapid association between the peptide and the bilayer, in a similar manner and timescale as the peptide-DMPC simulations described earlier. Representative structures of $EqtII_{1–32}$ peptide after binding to a 1:1 mixed DMPC:SM bilayer are shown in Figure 6(j,k). Similar to the DMPC simulations, initial interactions are formed between the N-terminus of the peptide (within 1 ns) with the lipid bilayer, followed by the C-terminus (~20 ns). Figure 6(k) illustrates the system at 70 ns, viewed along the bilayer normal. DMPC molecules are shown as blue spheres, while sphingomyelin molecules are shown as red spheres. The graphic illustrates a degree of phase separation between the two lipid types, with nanometre-scale domains ("nanodomains") composed primarily of DMPC or SM distributed throughout the simulated bilayer. The C-terminal part of the peptide exhibits preferential interaction with SM. This is more clearly manifested in a contact profile plot [Fig. 8(d)], which indicates that while the N-terminal side of the peptide interacts somewhat more favorably with DMPC phosphates (with contacts made via Ser1, Ala2, and Asp3, as opposed to only Ser1 for sphingomyelin), the C-terminal side (via Lys30 and Lys32) exhibits significantly greater numbers of contacts with sphingomyelin phosphates. Preferential interaction of the peptide with either DMPC or SM may contribute to its enhanced secondary structural persistence (discussed earlier) compared with that of a pure DMPC bilayer. The mixed bilayer thus imposes structural order on the peptide, due to its own intrinsic nanodomain order. The enhancement of structural order may in turn contribute to the enhanced activity of the peptide on PC:SM bilayers.[43]

CONCLUSIONS

We have applied SS NMR and MD computational simulations to examine the structure and DMPC:SM bilayer interactions of the N-terminal peptide (residues 1–32) of the highly soluble toxin EqtII. For the peptide in solution, the distances between specifically labeled nuclei in [^{19}F-para]Phe16-[1-^{13}C]Leu19 and [^{19}F-para]Phe16-[^{15}N]Leu23 analogs of $EqtII_{1–32}$ measured by REDOR in lyophilized powder were in agreement with published crystal and solution structures. However, in both DMPC and mixed DMPC:SM membrane environments, significant changes in the distances between the labeled amino acid pairs were observed, suggesting changes in helical content in this region in the presence of bilayers. Differences in REDOR-acquired peptide–lipid interatomic distances between pure DMPC and mixed DMPC:SM bilayers were also observed, which may be due to the greater affinity of EqtII for the latter. MD simulations of both $EqtII_{1–32}$ and EqtII indicated that the regions around the N-terminus and the aromatic and positively charged residues are highly flexible and contribute to membrane binding as well as undergoing changes in secondary structure during interaction with bilayers. Comparison of the water-solvated peptide structure, which is largely disordered, indicates that binding to a DMPC surface induces helix formation at residues ~16–24. The simulation results also indicate strong interaction between the peptide and the mixed DMPC:SM bilayer, with the C-terminus exhibiting preferential interaction with SM. The large portion of the peptide which maintains helical structure, coupled with a tendency to form a β-stranded N-terminal tail, may be a contributing factor to the greater membrane activity of the peptide against mixed PC:SM bilayers.

The appearance of similar structural and bilayer-binding characteristics in simulations with widely varying initial conformations lends credence to the notion that these phenomena are genuine features of $EqtII_{1–32}$-bilayer interactions. Our MD simulation results indicate persistent interactions with the lipid bilayer of the N-terminal region, as well as the aromatic and positively charged regions. These regions are known from previous studies to play a role in membrane interactions of EqtII. Thus, the overall mechanism of EqtII peptide and protein initial interaction with the DMPC bilayer, based on the contacts with phosphates and acyl chains which appear to be shared in common, may be summarized as follows: the initial binding event, driven by electrostatic attraction, appears to be between the N-terminus and the phosphate headgroups. Thereafter, the N- and C-termini both anchor the peptide to the bilayer. Further electrostatic interactions between Lys residues (which are located at the center and C-terminal regions of the peptide) and phosphate headgroups may serve to drive the peptide toward a roughly parallel orientation. Hydrophobic interactions may also be formed between various nonpolar residues and the upper segments of the acyl chains, such as Gly11 and Ala12, as suggested by **pep-wat-DMPC**. The latter interactions may, given a longer timescale, disrupt the bilayer core sufficiently for full peptide and protein insertion. In summary, the results obtained from our SS NMR and MD studies of the interaction of the N-terminus of EqtII with phospholipid bilayers may be indicative of the first step in the conformational changes required for the permeation and subsequent disruption of the membrane due to the binding of the peptide.

ACKNOWLEDGMENTS

YHL thanks the Oxford Supercomputing Centre for provision of computational resources for performing MD simulations, through the Bionanotechnology IRC. The authors like to thank Alison Drechsler for helpful discussions.

REFERENCES

1. Maček P, Lebez D. Isolation and characterization of three lethal and hemolytic toxins from the sea anemone. Toxicon 1988;26:441–451.
2. Zorec R, Tester M, Maček P, Mason WT. Cytotoxicity of equinatoxin II from the sea anemone *Actinia equina* involves ion channel formation and an increase in intracellular calcium activity. J Membr Biol 1990;131:11–22.
3. Belmonte G, Pederzolli C, Maček P, Menestrina G. Pore formation by the sea anemone cytolysin equinatoxin II in red blood cells and model lipid membranes. J Membr Biol 1993;118:243–249.
4. Maček P, Belmonte G, Pederzolli C, Menestrina G. Mechanism of action of equinatoxin II, a cytolysin from the sea anemone *Actinia equina L.* belonging to the family of actinoporins. Toxicology 1994; 87:205–227.
5. Anderluh G, Macek P. Cytolytic peptide and protein toxins from sea anemones (Anthozoa: Actiniaria). Toxicon 2002;40:111–124.
6. Alegre-Cebollada J, Oñaderra M, Gavilanes JG, Martinez Del Pozo A. Sea anemone actinoporins: the transition from a folded soluble state to a functionally active membrane-bound oligomeric pore. Curr Protein Pept Sci 2007;8:558–572.
7. Athanasiadis A, Anderluh G, Maček P, Turk D. Crystal structure of the soluble form of equinatoxin II, a pore-forming toxin from the sea anemone *Actinia equina.* Structure 2001;9:341–346.
8. Hinds MG, Zhang W, Anderluh G, Hansen PE, Norton RS. Solution structure of the eukaryotic pore-forming cytolysin equinatoxin II: implications for pore formation. J Mol Biol 2002;315:1219–1229.
9. Drechsler A, Potrich C, Sabo JK, Frisanco M, Guella G, Serra MD, Anderluh G, Separovic F, Norton RS. Structure and activity of the N-terminal region of the eukaryotic cytolysin equinatoxin II. Biochemistry 2006;45:1818–1828.
10. Anderluh G, Barlič A, Potrich C, Macek P, Menestrina G. Lysine 77 is a key residue in aggregation of equinatoxin II, a pore-forming toxin from sea anemone *Actinia equina.* J Membr Biol 2000;173:47–55.
11. Anderluh G, Razpotnik A, Podlesek Z, Maček P, Separovic F, Norton RS. Interaction of the eukaryotic pore-forming cytolysin equinatoxin II with model membranes: 19F NMR studies. J Mol Biol 2005;347:27–39.
12. Killian JA, Von Heijne G. How proteins adapt to a membrane-water interface. Trends Biochem Sci 2000;25:429–434.
13. Kennedy MW, Beauchamp J. Sticky-finger interaction sites on cytosolic lipid-binding proteins? Cell Mol Life Sci 2000;57:1379–1387.

14. Wimley WC, White SH. Experimentally determined hydrophobicity scale for proteins at membrane interfaces. Nat Struct Biol 1996;3: 842–848.
15. Hong Q, Qutierrez K, Podelsek Z, Maček P, Turk D, Gonzales-Manas JM, Lakey JH, Anderluh G. Two-step membrane binding of equinatoxin II, a pore-forming toxin from the sea anemone, involves an exposed aromatic cluster and a flexible helix. J Biol Chem 2002;277:41916–41924.
16. Poklar N, Fritz J, Maček P, Vesnaver G, Chalikian TV. Interaction of the pore-forming protein equinatoxin II with model lipid membranes: a calorimetric and spectroscopic study. Biochemistry 1999; 38:14999–15008.
17. Menestrina G, Cabiaux V, Tejuca M. Secondary structure of sea anemone cytolysins in soluble and membrane bound form by infrared spectroscopy. Biochem Biophys Res Commun 1999;254:174–180.
18. Anderluh G, Barlic A, Podlesek Z, Maček P, Pungerčar J, Gubenšek F, Zecchini ML, Serra MD, Menestrina G. Cysteine-scanning mutagenesis of an eukaryotic pore-forming toxin from sea anemone: topology in lipid membranes. Eur J Biochem 1999;263:128–136.
19. Malovrh P, Barlič A, Podlesek Z, Maček P, Menestrina G, Anderluh G. Structure-function studies of tryptophan mutants of equinatoxin II, a sea anemone pore-forming protein. Biochem J 2000;346:223–232.
20. Gullion T, Schaefer J. Rotational echo double-resonance NMR. J Magn Reson 1989;81:196–200.
21. Gullion T, Schaefer J. Detection of weak heteronuclear dipolar coupling by rotational-echo double resonance. Adv Magn Reson 1989; 13:57–83.
22. Bak M, Rasmussen JT, Nielsen NC. SIMPSON: a general simulation program for solid-state NMR Spectroscopy. J Magn Reson 2000; 147:296–330.
23. Berendsen HJC, Postma JPM, Gunsteren WFV, Hermans J. Interaction models for water in relation to protein hydration. In: Pullman B, editor. Intermolecular forces. Dordrecht: Reidel; 1981. p 331.
24. Van Gunsteren WF, Krüger P, Billeter SR, Mark AE, Eising AA, Scott WRP, Hüneberg PH, Tironi IG. Biomolecular simulation: the GROMOS96 manual and user guide. Zurich, Switzerland: Biomos, Groningen and Hochsuchulverlag AG, Germany and er ETH Zürich; 1996.
25. Lindahl E, Hess B, Van Der Spoel D. Gromacs 3.0: a package for molecular simulation and trajectory analysis. J Mol Model 2001;7: 306–317.
26. Berger O, Edholm O, Jahnig F. Molecular dynamics simulations of a fluid bilayer of dipalmitoylphosphatidylcholine at full hydration, constant pressure, and constant temperature. Biophys J 1997;72: 2002–2013.
27. Chiu SW, Vasudevan S, Jakobsson E, Mashl RJ, Scott HL. Structure of sphingomyelin bilayers: a simulation study. Biophys J 2003;85: 3624–3635.
28. Berendsen HJC, Postma JPM, Van Gunsteren WF, Dinola A, Haak JR. Molecular dynamics with coupling to an external bath. J Chem Phys 1984;81:3684–3690.
29. Darden T, York D, Pedersen L. Particle mesh Ewald. An N-log(N) method for Ewald sums in large systems. J Chem Phys 1993;98: 10089–10092.
30. Hess B, Bekker H, Berendsen HJC, Fraaije JGEM. LINCS: a linear constraint solver for molecular simulations. J Comput Chem 1997; 18:1463–1472.
31. Kabsch W, Sander C. Dictionary of protein secondary structure: pattern recognition of hydrogen-bonded and geometrical features. Biopolymers 1983;22:2577–2637.
32. Humphrey W, Dalke A, Schulten K. VMD: visual molecular dynamics. J Mol Graph 1996;14:33–38.
33. Seavey BR, Farr EA, Westler WM, Markley JL. A relational database for sequence-specific protein NMR data. J Biomol NMR 1991;1: 217–236.
34. Ulrich EL, Akutsu H, Doreleijers JF, Harano Y, Ioannidis YE, Lin J, Livny Mm S, Maziuk D, Miller Z, Nakatani E, Schulte CF, Tolmie DE, Kent Wenger R, Yao H, Markley JL. BioMagResBank. Nucleic Acids Res 2008;36:D402–D408.
35. Grage SL, Watts A. Applications of REDOR for distance measurements in biological solids. Ann Rep NMR Spectrosc 2007;60:191–228.
36. Demmers JA, Van Duijn E, Haverkamp J, Greathouse DV, Heck AJ, Killian JA. A. Interfacial positioning and stability of transmembrane peptides in lipid bilayers studied by combining hydrogen/deuterium exchange and mass spectrometry. J Biol Chem 2001;276:34501–34508.
37. Bonev BB, Lam Y-H, Anderluh G, Watts A, Norton RS, Separovic F. Effects of the eukaryotic pore-forming cytolysin equinatoxin II on lipid membranes and the role of sphingomyelin. Biophys J 2003; 84:2382–2392.
38. Malovrh P, Viero G, Dalla Serra M, Podlesek Z, Lakey JH, Maček P, Menestrina G, Anderluh G. A novel mechanism of pore formation: membrane penetration by the N-terminal amphipathic region of equinatoxin. J Biol Chem 2003;278:22678–22685.
39. Barlic A, Gutiérrez-Aguirre I, Caaveiro JM, Cruz A, Ruiz-Argüello MB, Pérez-Gil J, González-Mañas JM. Lipid phase coexistence favors membrane insertion of equinatoxin-II, a pore-forming toxin from *Actinia equina*. J Biol Chem 2004;279:34209–34216.
40. Bakrač B, Gutiérrez-Aguirre I, Podlesek Z, Sonnen AF-P, Gilbert RJC, Maček P, Lakey JH, Anderluh G. Molecular determinants of sphingomyelin specificity of a eukaroytic pore forming toxin. J Biol Chem 2008;283:18665–18677.
41. Schőn P, Garcia-Saez AJ, Malovrh P, Bacia K, Anderluh G, Schwille P. Equinatoxin II permeabilizing activity depends on the presence of sphingomyelin and lipid phase coexistence. Biophys J 2008;95: 691–698.
42. Caaveiro JMM, Echanbe I, Gutierres-Aguirre I, Nieva JL, Arrondo JLR, Gonzalez-Manas JM. Differential interaction of equinatoxin II with model membranes in response to lipid composition. Biophys J 2001;80:1343–1353.
43. Kim SJ, Cegelski L, Studelska DR, O'connor RD, Mehta AK, Schaefer J. Rotational-echo double resonance characterization of vancomycin binding sites in *Staphylococcus aureus*. Biochemistry 2002;41: 6967–6977.
44. Jie L, Larisa A, Ronald Jackups J. The membrane–water interface region of membrane proteins: structural bias and the anti-snorkeling effect. Trends Biochem Sci 2005;30:355–357.